Transient Protein Interactions Studied by NMR Spectroscopy: The Case of Cytochrome *c* and Adrenodoxin[†]

Jonathan A. R. Worrall,[‡] Wolfgang Reinle,[§] Rita Bernhardt,[§] and Marcellus Ubbink*[,‡]

Gorlaeus Laboratories, Leiden Institute of Chemistry, Leiden University, P.O. Box 9502, 2300 RA Leiden, The Netherlands, and Naturwissenschaftlich-Technische Fakultät III, Fachrichtung 8.8-Biochemie, Universität des Saarlandes, Saarbrücken, Germany

Received February 21, 2003; Revised Manuscript Received April 14, 2003

ABSTRACT: The interaction between yeast iso-1-cytochrome *c* (C102T) and two forms of bovine adrenodoxin, the wild type and a truncated form comprising residues 4−108, has been investigated using a combination of one- and two-dimensional heteronuclear NMR spectroscopy. Chemical shift perturbations and line broadening of amide resonances in the [^{15}N,^{1}H]HSQC spectrum for both ^{15}N-labeled cytochrome *c* and adrenodoxin in the presence of the unlabeled partner protein indicate the formation of a transient complex, with a K_a of $(4 \pm 1) \times 10^4$ M^{-1} and a lifetime of <3 ms. The perturbed residues map over a large surface area for both proteins. For cytochrome *c*, the dominating effects are located around the exposed heme edge but with other areas also affected upon formation of the complex. In the case of adrenodoxin, effects are seen in both the recognition and core domains, with the largest perturbations in the recognition domain. These results indicate that the complex has a dynamic nature, with delocalized binding of cytochrome *c* on adrenodoxin. A comparison with other transient complexes of redox proteins places this complex between well-defined complexes such as the cytochrome *c*−cytochrome *c* peroxidase complex and entirely dynamic complexes such as the cytochrome b_5−myoglobin complex.

Electron transfer between proteins, as observed in cellular metabolism, generally requires formation of complexes with a high turnover rate. These protein−protein complexes are characterized by a lifetime on the order of milliseconds and equilibrium dissociation constants (K_ds) in the millimolar to micromolar range (*1*). These characteristics have led to the term transient complexes. A fundamental question is how transient complexes achieve a high turnover rate and yet react with sufficient specificity for the ET[1] step to be efficient. Complexes of redox proteins can be formed not only between physiological partners but also between nonphysiological partners. Nonphysiological partners can demonstrate fast ET (*2, 3*) and K_d values in the same range as that of the physiological partner, for example, between mitochondrial cytochrome *c* and chloroplast plastocyanin (*4*−*7*). Recent studies (*8*−*11*) on various physiological as well as nonphysiological ET complexes suggest that specificity has been "sacrificed" to achieve high turnover rates. This is apparent in particular for the complex of cytochrome b_5 and myoglobin, where no specific complex appears to be formed, but rather a complex existing as a dynamic ensemble of orientations (*9, 10, 12*−*14*).

Adrenodoxin (128 residues; $M_r = 14.4$ kDa) is a member of the vertebrate-type [2Fe-2S] ferredoxins and contains a single [2Fe-2S] cluster with each iron tetrahedrally coordinated by two cysteinyl sulfurs and two μ-sulfido ligands (*15*). Adx acts as an electron shuttle in the mitochondrial ET chain responsible for the production of steroid hormones in mammals. It receives electrons from a NADPH-dependent adrenodoxin reductase (AdR) and donates them to cytochrome P450scc (CYP11A1), which in the adrenals catalyzes the side chain cleavage of cholesterol, or to cytochromes of the CYP11B family, involved in the formation of cortisol and aldosterone (*16*).

Adx contains a stretch of amino acids (residues 109−128) which is absent in plant-type ferredoxins. This C-terminal "tail" of Adx has been proposed to be highly flexible and disordered (*17*). In the crystal structure of the wild-type protein, electron density is observed up to residue 111 (*18*), whereas in the crystal structure of the cross-linked wild-type Adx−AdR complex, the tail is structured up to residue 117 and makes contact with the reductase (*19*). A truncated form (comprising residues 4−108) of Adx demonstrates a decreased affinity for the AdR, but an electron transfer rate more efficient than that of the wild-type protein (*15*). Moreover, truncation of Adx enhances the efficiency of ET to CYP11B1 and improves the binding to cytochrome P450 (*20, 21*).

In vitro ET from AdR to Adx is often monitored by fast subsequent ET from Adx to mitochondrial cytochrome *c*

[†] This work was supported by TMR *Haemworks* Contract FMRX-CT98-0218 and the Deutsche Forschungsgemeinschaft (Grant Be1343/12-1).

* To whom correspondence should be addressed. Phone: +31 71 527 4628. Fax: +31 71 527 4593. E-mail: m.ubbink@chem.leidenuniv.nl.

[‡] Leiden University.

[§] Universität des Saarlandes.

[1] Abbreviations: Adx, bovine adrenodoxin; AdR, bovine adrenodoxin reductase; cyt *c*, yeast iso-1-cytochrome *c* with T−5A and C102T mutations; *wt* Adx, full-length bovine adrenodoxin with an S1M mutation; Adx(4−108), truncated mutant of bovine adrenodoxin; HSQC, heteronuclear single-quantum coherence; NMR, nuclear magnetic resonance; TSP, sodium 3-(trimethylsilyl)-d_4-propionate; DTT, dithiothreitol; 1D, one-dimensional; 2D, two-dimensional; C*c*P, yeast cytochrome *c* peroxidase; cyt b_5, bovine cytochrome b_5; Mb, bovine myoglobin; cyt *f*, cytochrome *f*; Pc, plastocyanin; ET, electron transfer.

10.1021/bi0342968 CCC: $25.00
Published on Web 05/21/2003

(*22*−*25*). The hemoprotein cytochrome *c* is used in this reaction as a model for the hemoprotein cytochrome P450. Although this represents a nonphysiological reaction, it is widely used because the one-electron transfer from AdR to Adx is the slowest and thus the rate-limiting step in the reaction (*26*). The fact that Adx and cytochrome *c* show fast ET suggests that a complex is formed. We have investigated the interaction of Adx and cytochrome *c* in solution using NMR spectroscopy.

NMR spectroscopy provides a fast method for analyzing weak protein−protein interactions (*27*), and is therefore highly amenable to the study of transient protein complexes. Using isotope labeling of one protein (usually with ^{15}N) and titrating in the unlabeled partner protein, chemical shift changes in a [^{15}N,^{1}H]HSQC spectrum can be observed, provided that the dissociation rate constant for the complex, k_{off}, is sufficiently high (>200 s^{-1}) (*28*−*34*). These chemical shift changes along with increases in line widths contain information concerning the dynamics within the complex (*8*, *10*). Moreover, from the chemical shift changes upon complex formation the stoichiometry of binding and the equilibrium binding constant can be determined, and the interaction site(s) can be mapped.

In our previous studies with transient complexes, chemical shift maps for only one of the proteins in the complex could be obtained (*8*, *10*, *11*, *33*, *34*). Here however, both proteins have been labeled with ^{15}N, enabling the analysis of the effects of complex formation on both proteins. Two forms of bovine Adx, the wild type and the truncated form, Adx(4−108), with yeast iso-1-cytochrome *c* (C102T) were analyzed. The results indicate the presence of dominant sites for binding on both proteins, but also some degree of mobility within the complex, resulting in interactions of cyt *c* with a large part of Adx. These results allow comparisons to be drawn with other transient ET complexes of both physiological and nonphysiological origin in which cyt *c* is a partner (*7*, *11*, *34*).

MATERIALS AND METHODS

Protein Isolation. Isotope-enriched ^{15}N-labeled and unlabeled yeast cyt *c* (C102T) were expressed in *Escherichia coli* and purified as previously described (*35*, *36*). Adrenodoxin was produced in *E. coli* BL21 using the plasmid pKKHC containing either *wt* Adx or the truncated mutant Adx(4−108), which is missing amino acids 1−3 and 109−128 (*21*). The cells were grown in M9 minimal medium containing $^{15}NH_4Cl$ as the sole nitrogen source, supplemented with $FeCl_3$ (50 μM), 250 ppm thiamine, and trace amounts of B, Mn, Zn, Mo, Cu, and Co salts. The cell pellet was frozen at −20 °C prior to purification. For purification, the thawed cell pellet was lysed by sonication. The supernatant was first loaded onto an anion exchange column (TSKgel DEAE-TOYOPEARL, 650S-TOSOH Corp., Tokyo, Japan). The brown fractions, containing Adx, were pooled and concentrated using an Amicon Centriprep centrifugal filter device and then further purified using gel filtration (Sephadex G-50 fine, Pharmacia Biotech). The purity index (A_{414}/A_{276}) was 0.9, an indication of highly pure isolated, labeled proteins.

Preparation of NMR Samples. Oxidized *wt* Adx and Adx(4−108) were exchanged into 20 mM sodium phosphate (pH 7.4) by ultrafiltration methods (Amicon; YM5 membrane). Ferrous cyt *c* was prepared in an analogous way except an excess (2−3-fold) of sodium ascorbate was added prior to buffer exchange. Protein concentrations were determined optically according to the absorbance peak at 550 nm (ϵ = 27.5 mM^{-1} cm^{-1}) for ferrous cyt *c* (*37*) and at 414 nm (ϵ = 9.8 mM^{-1} cm^{-1}) for oxidized Adx (*38*).

NMR samples of ^{15}N-labeled and unlabeled cyt *c* ranged in concentration from 1.4 to 3.6 mM, and for ^{15}N-labeled and unlabeled Adx concentrations in the range of 0.58−1.0 mM were used. All NMR samples contained 1 mM DTT and 6% D_2O for lock and 100 μM TSP and [^{15}N]acetamide as internal references. The pH for all protein samples was adjusted to 7.40 ± 0.05, and the solutions were degassed by blowing argon over the surface.

Backbone Amide NMR Assignments. All NMR experiments were performed on a Bruker DMX600 spectrometer operating at 285 K equipped with a TXI-Z-GRAD (^{1}H, ^{13}C, ^{15}N) probe. For sequence-specific assignment of backbone amide resonances of *wt* Adx and Adx(4−108), two-dimensional (2D) homonulear NOESY and TOCSY and heteronuclear 2D [^{15}N,^{1}H]HSQC, 2D [^{15}N,^{1}H]HSQC-NOESY, and 2D [^{15}N,^{1}H]HSQC-TOCSY spectra were recorded. Data processing was performed in AZARA (available from ftp://ftp.bio.cam.ac.uk/pub/azara), and resonance assignment was performed in ANSIG (*39*, *40*) on the basis of assignments at pH 7.4 and 300 K (*41*).

NMR Titration Experiments. Four sets of titration data were recorded each with the addition of microliter aliquots of cyt *c* into an initial Adx sample. Before the start of each titration, reference spectra were recorded with either [^{15}N]-cyt *c* or [^{15}N]Adx. For the first titration, an initial *wt* Adx concentration of 0.74 mM was used with a final molar ratio of 1:2.5 (*wt* Adx:[^{15}N]cyt *c*). In the second, 0.96 mM Adx(4−108) was used with a final molar ratio of 1:1.25 [Adx(4−108):[^{15}N]cyt *c*]. In the third, 0.85 mM [^{15}N]Adx was used with a final molar ratio of 1:2.0 ([^{15}N]*wt* Adx:cyt *c*). Finally, an initial [^{15}N]Adx(4−108) concentration of 0.58 mM with a final molar ratio of 1:2.2 [[^{15}N]Adx(4−108):cyt *c*] was used. Before and after each titration step, the pH of the sample was verified and adjusted if necessary. All titration experiments were carried out using one-dimensional (1D) proton and 2D [^{15}N,^{1}H]HSQC (*42*) spectra. Data processing of the 1D proton spectra was performed in XWINNMR, and the [^{15}N,^{1}H]HSQC spectra were processed in AZARA. Chemical shift perturbations of ^{15}N and ^{1}H nuclei for the respective ^{15}N-labeled proteins upon interaction with their unlabeled partner were analyzed by overlaying the spectra of the bound form with the free protein in the assignment program ANSIG (*39*, *40*).

Titration Curves and Average Amide Chemical Shift. Chemical shift changes of amide ^{1}H or ^{15}N nuclei were plotted against the molar ratio of cyt *c* and Adx. A two-parameter nonlinear least-squares fit of the data using a one-site binding model which corrects for dilution effects (*43*)

$$\Delta\delta_{binding} = \frac{1}{2}\Delta\delta_{max}(A - \sqrt{A^2 - 4R}) \qquad (1)$$

$$A = 1 + R + \frac{PR + C}{PCK_a}$$

was performed in the program Origin version 6.0 (Microcal Software, Northampton, MA). In eq 1, R is the [cyt *c*]:[[^{15}N]-

Adx] ratio, $\Delta\delta_{binding}$ is the chemical shift change relative to the free protein when titrating in the partner protein, $\Delta\delta_{max}$ is the chemical shift change for $R \rightarrow \infty$, P and C are the concentrations of [^{15}N]Adx at the start of the titration and of the stock cyt *c* solution, respectively, and K_a is the binding constant. For data in which cyt *c* resonances were observed ([^{15}N]cyt *c*), R is replaced in eq 1 with $1/R$ and $\Delta\delta_{max}$ is replaced with $\Delta\delta_0$, the chemical shift change for nuclei of [^{15}N]cyt *c* for $R \rightarrow 0$.

For a comparative representation between the different sets of titration data, the amide chemical shifts were extrapolated to the 100% bound form by estimating from the titration data the percentage of bound protein at a stoichiometry of 1:1. The average amide chemical shift perturbation ($\Delta\delta_{avg}$) was then derived from

$$\Delta\delta_{avg} = \sqrt{\frac{(\Delta\delta N/5)^2 + \Delta\delta H^2}{2}} \qquad (2)$$

in which $\Delta\delta$N represents the change in the chemical shift of the amide nitrogen and $\Delta\delta$H represents the change in the chemical shift in the amide proton (*44*).

RESULTS

Backbone Amide Assignments of Cyt c and Adx. Amide assignments for ferrous cyt *c* from previous work (*34*) were used with amides −4, 3, 4, 34, 57, 60, 83, 84, and 87 out of a possible 104 non-proline residues being unassigned under the conditions presented here due to either spectral overlap or exchange with bulk solvent. In this study, two forms of oxidized Adx were used: *wt* Adx, residues 1−128, where the first amino acid is changed from serine to methionine, and a shortened construct [Adx(4−108)], where the highly flexible C-terminal tail (*17*), residues 109−128, and residues 1−3 were absent (*21*). Assignments of the amide nuclei of *wt* Adx were aided by known literature assignments (*41*), with Adx(4−108) being assigned in the work presented here (Table S1). From a total of 127 and 103 non-proline residues for *wt* Adx and Adx(4−108), respectively, 50 amide resonances remained unassigned for *wt* Adx and 25 for Adx-(4−108). In the oxidized form of Adx, both the high-spin Fe^{III} ions are antiferromagnetically coupled in the ground state ($S = 0$), with the thermal population of excited states at physiological temperatures accounting for the paramagnetic effects observed in the NMR spectra (*45*). Therefore, for both *wt* Adx and Adx(4−108), residues situated in the vicinity of the Cys ligand binding loops remained unassigned (44−56 and 90−94) due to fast paramagnetic relaxation. Furthermore, residues 109−128 (forming the flexible C-terminal tail) and residues 2−4, 25, 26, 32, 37, 62, 65, 69, 83, and 85 for *wt* Adx and 4, 22, 32, 37, 71, 78, and 101 for Adx(4−108) remained unassigned in this work.

Titration of [^{15}N]Cyt c to Adx and Chemical Shift Mapping. Ferrous [^{15}N]cyt *c* was titrated into a sample of oxidized Adx, and a series of 2D [^{15}N,^{1}H]HSQC spectra were recorded. Experiments with both *wt* Adx and Adx(4−108) were carried out. In both cases, a general broadening of the resonances and significant chemical shift changes ($\Delta\delta_{binding}$) for the amide nuclei of cyt *c* were observed (Figure 1A). Increases in the line width at half-height in the proton dimension of 26 and 21 Hz were observed upon interaction with *wt* Adx and Adx(4−108), respectively. The observed line broadening of the perturbed cyt *c* peaks is no larger than that of the unaffected peaks in the bound form. This behavior is characteristic of a fast exchange regime on the NMR time scale ($k_{off} > 300\ s^{-1}$), yielding a single averaged resonance for the perturbed amide peaks of cyt *c* upon formation of a complex with Adx. Addition of excess [^{15}N]cyt *c* caused the perturbed peaks to move back toward the positions of the free form. The $\Delta\delta_{binding}$ values for several perturbed [^{15}N]-cyt *c* resonances (both ^{1}H and ^{15}N) are plotted against the molar ratio of [^{15}N]cyt *c* and Adx in Figure 1 (panels B and C) and fitted globally to a 1:1 binding model (eq 1). A binding constant (K_a) of $(4 \pm 1) \times 10^4\ M^{-1}$ was obtained for titration to both *wt* Adx and Adx(4−108), indicating that at the protein concentrations that were used approximately 80% of cyt *c* is bound to Adx at a molar ratio of 1.0.

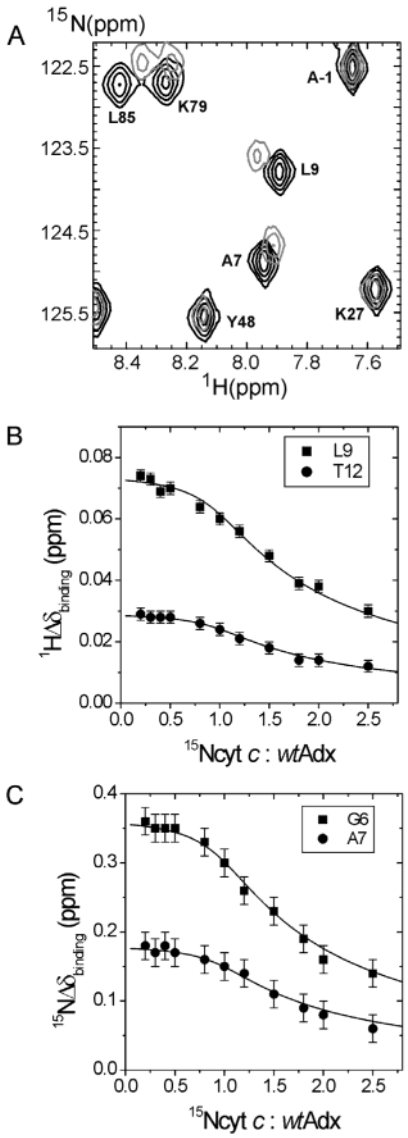

FIGURE 1: (A) Overlay of part of the [^{15}N,^{1}H]HSQC spectra of yeast ferrous cyt *c* in the free form (black) and bound to *wt* Adx (gray). The [^{15}N]cyt *c*:*wt* Adx ratio was 0.5:1 in 20 mM sodium phosphate at pH 7.4 and 285 K. Examples of titration curves for the titration of ferrous [^{15}N]cyt *c* to *wt* Adx. The chemical shift changes ($\Delta\delta_{binding}$) for the H^N (B) and N^H (C) atoms of cyt *c* residues are plotted as a function of the [^{15}N]cyt *c*:Adx ratio and fitted globally using eq 1 for a 1:1 complex, yielding a K_a of $(4 \pm 1) \times 10^4\ M^{-1}$.

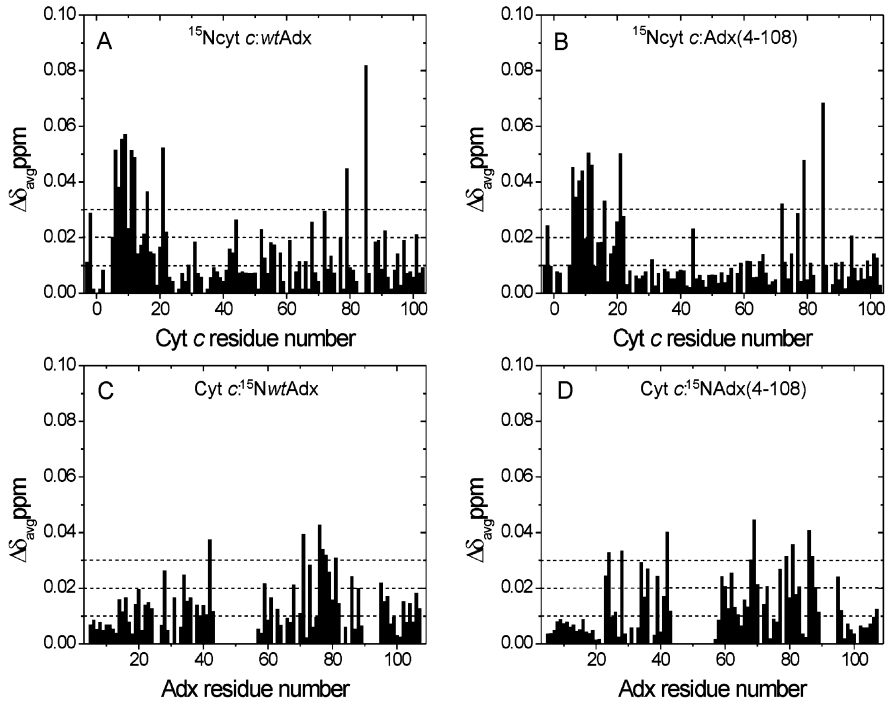

FIGURE 2: Changes in the average amide chemical shift ($\Delta\delta_{avg}$) extrapolated to 100% bound experienced by [^{15}N]cyt *c* upon formation of a complex with (A) *wt* Adx and (B) Adx(4−108) and the $\Delta\delta_{avg}$ for [^{15}N]*wt* Adx (C) and [^{15}N]Adx(4−108) (D) experienced upon formation of a complex with cyt *c*. Dashed lines indicate the $\Delta\delta_{avg}$ categories (≥0.03 ppm for large, ≥0.02 ppm for medium, ≥0.01 ppm for small, and <0.01 ppm for insignificant) for chemical shift mapping onto surface representations of the two proteins.

The backbone amide chemical shifts for cyt *c* at a molar ratio of 1.0 with Adx were extrapolated to 100% bound, and the average amide chemical shift ($\Delta\delta_{avg}$) was calculated from eq 2. Forty-four cyt *c* amides are significantly affected upon titration to *wt* Adx and 37 upon titration to Adx(4−108) (Figure 2A,B). In Figure 3, the $\Delta\delta_{avg}$ values for cyt *c* upon interaction with both forms of Adx have been color-coded according to the size of their shift, and mapped onto surface representations of the protein. The majority of the affected amides lie on the front face of cyt *c* surrounding the exposed heme edge, with the amides of G6, A7, T8, L9, K11, T12, Q16, E21, K79, and L85, exhibiting the largest $\Delta\delta_{avg}$ values (≥0.03 ppm) for formation of a complex with *wt* Adx, with the addition of K72 for formation of a complex with Adx-(4−108). At the rear of the protein, binding effects are also observed. For formation of a complex with *wt* Adx, the effects at the rear of cyt *c* are more extensive than with Adx-(4-108), but the effects are just above the significance limit.

Titration of Cyt c to [^{15}N]Adx and Chemical Shift Mapping. As with the previous [^{15}N]cyt *c* titrations, addition of microliter aliquots of ferrous cyt *c* to oxidized [^{15}N]Adx led to a general increase in the line broadening and a significant number of $\Delta\delta_{binding}$ effects for ^{15}N and ^{1}H nuclei in the [^{15}N,^{1}H]HSQC spectra for both forms of [^{15}N]Adx (Figure 4A). Again, this is consistent with a fast exchange process on the NMR time scale. For some significantly perturbed peaks, $\Delta\delta_{binding}$ values were plotted as a function of the molar ratio of cyt *c* and [^{15}N]Adx, and fitted globally to a 1:1 binding model (eq 1). The fits are consistent with the previous reverse titration data for [^{15}N]cyt *c* with a K_a of $(3 \pm 1) \times 10^4$ M^{-1}.

In Figure 2 (panels C and D), the $\Delta\delta_{avg}$ amide chemical shifts extrapolated to 100% bound for [^{15}N]Adx upon interaction with cyt *c* are plotted as a function of Adx residue number. For *wt* Adx, 41 amides are affected, while for Adx-(4−108), 37 are affected. The perturbed Adx resonances have been mapped in accordance with the size of their chemical shift change upon formation of a complex with cyt *c* onto the respective crystal structures of Adx in Figure 5.

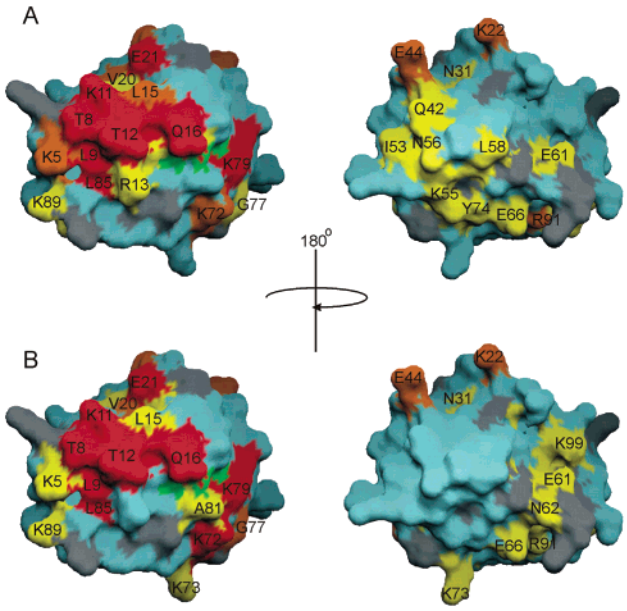

FIGURE 3: Chemical shift mapping of cyt *c* in the presence of (A) *wt* Adx and (B) Adx(4−108). Surface representations of ferrous cyt *c* (PDB entry 1YCC) (*46*) were generated using GRASP version 1.3 (*47*). Residues for which a $\Delta\delta_{avg}$ was calculated are color-coded according to the categories in Figure 2: red for ≥0.03 ppm, orange for ≥0.02 ppm, yellow for ≥0.01 ppm, and blue for <0.01 ppm. Unassigned and proline residues are in gray, and the heme is colored green. Residues are identified with the single-letter amino acid code, and the surfaces on the right have been rotated 180° around the vertical axis, with respect to those on the left.

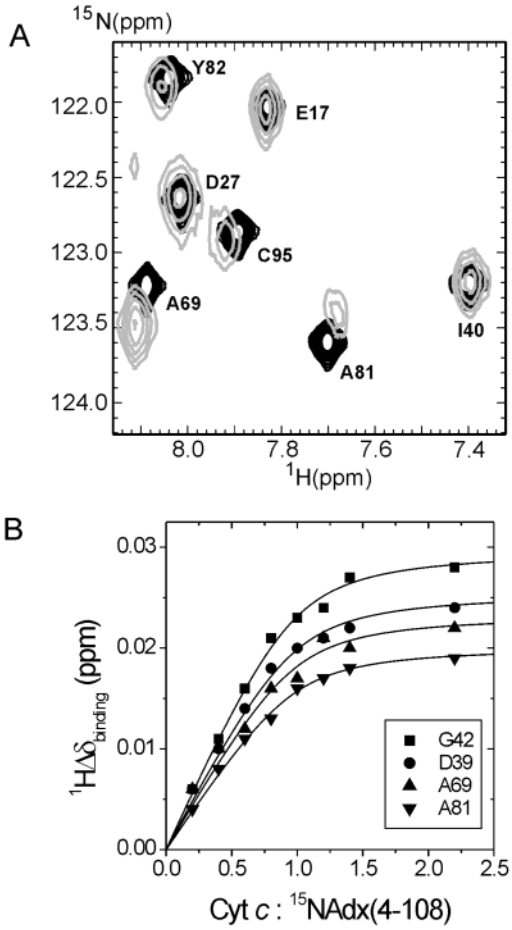

FIGURE 4: (A) Overlay of part of the [^{15}N,^{1}H]HSQC spectra of bovine Adx(4−108) in the free form (black) and bound to ferrous cyt *c* (gray). The cyt *c*:Adx ratio was 2.2:1 in 20 mM sodium phosphate at pH 7.4 and 285 K. (B) Examples of titration curves for the titration of ferrous cyt *c* to [^{15}N]Adx(4−108), with the chemical shift changes ($\Delta\delta_{binding}$) for H^N resonances of Adx(4−108) plotted as a function of the cyt *c*:[^{15}N]Adx ratio and fitted globally using eq 1 for a 1:1 complex, yielding a K_a of $(3 \pm 1) \times 10^4$ M^{-1}. The margin of error in the data is equivalent to the size of the symbols.

The polypeptide chain of Adx is organized into two domains (*48*). The first is a large core domain, harboring the iron−sulfur cluster and spanning residues 5−55 and 91−108. The second domain forms a large hairpin and comprises residues 56−90. The latter domain bears the key residues for recognition of AdR and CYP11A1 and is termed the recognition domain. The chemical shift maps display patches of residues affected in both the core and recognition domain, with the majority of the amides with the largest $\Delta\delta_{avg}$ values (≥0.03 ppm) situated in the latter. The amides of G42, T71, D76, M77, L78, and A81 show the largest $\Delta\delta_{avg}$ values for *wt* Adx, and K24, S28, G42, E68, A69, D79, A81, D86, and R87 demonstrate the largest $\Delta\delta_{avg}$ values for Adx(4−108).

For *wt* Adx, a number of sharp resonances are observed in the [^{15}N,^{1}H]HSQC spectra which from previous assignments are known to arise form the flexible C-terminal tail of the protein (*41*). Line broadening (5 Hz) and chemical shift changes are observed for a small number of tail peaks in the HSQC spectra of *wt* Adx upon formation of a complex (Figure 6). These observations suggest that the tail is in some manner involved in formation of a complex with cyt *c*, although without affecting the affinity of the overall binding.

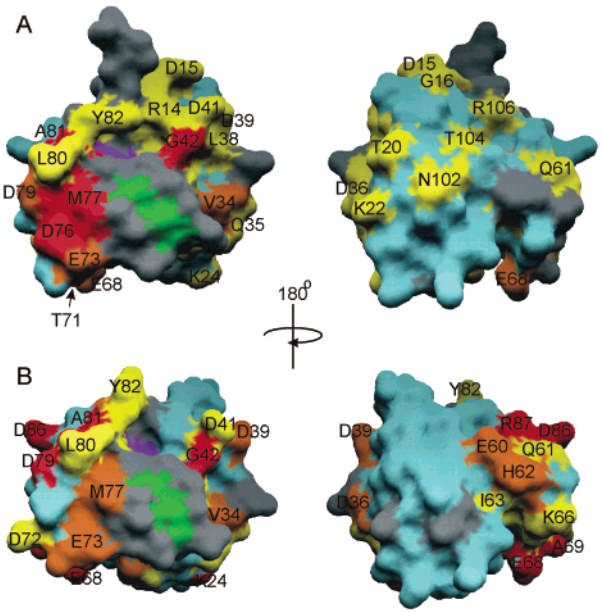

FIGURE 5: Chemical shift mapping in the presence of ferrous cyt *c* for (A) *wt* Adx and (B) Adx(4−108). Surface representations of *wt* Adx (PDB entry 1CJE) (*18*) and Adx(4−108) (PDB entry 1AYF) (*48*) were generated using GRASP version 1.3 (*47*). Residues for which a $\Delta\delta_{avg}$ was calculated are color-coded according to the categories in Figure 2: red for ≥0.03 ppm, orange for ≥0.02 ppm, yellow for ≥0.01 ppm, and blue for <0.01 ppm. Unassigned and proline residues are in gray; purple represents the position of His56, and green indicates two of the active site cysteine residues (Cys46 and Cys52). Residues are identified with the single-letter amino acid code, and the surfaces on the right have been rotated 180° around the vertical axis, with respect to those on the left.

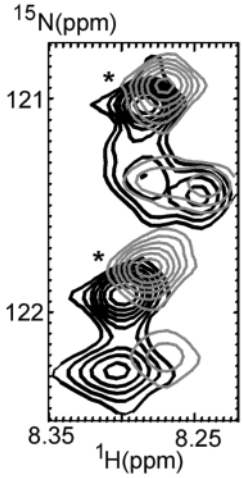

FIGURE 6: Overlay of part of the [^{15}N,^{1}H]HSQC spectra of bovine *wt* Adx in the free form (black) and in complex with ferrous cyt *c* (gray). Asterisks mark the unassigned tail peaks which are perturbed upon complex formation.

1D Adx:cyt c NMR Titrations. It is unclear whether the hydrophobic area surrounding the active site binding loop is involved in complex formation, due to the paramagnetism of the iron−sulfur cluster. A clue that suggests the active site senses the binding of cyt *c* arises form the one-dimensional ^{1}H spectrum of Adx. Here two distinct downfield-shifted signals are observed (Figure 7A). These have been assigned to $H_{\delta 1}$ of His56 and H_{γ} of Ser88 (*49*). The downfield position of the latter proton is due to its direct H-bond involvement with the unprotonated $N_{\epsilon 2}$ of His56 (*48*). His56 is conserved in all vertebrate-type ferredoxins (except

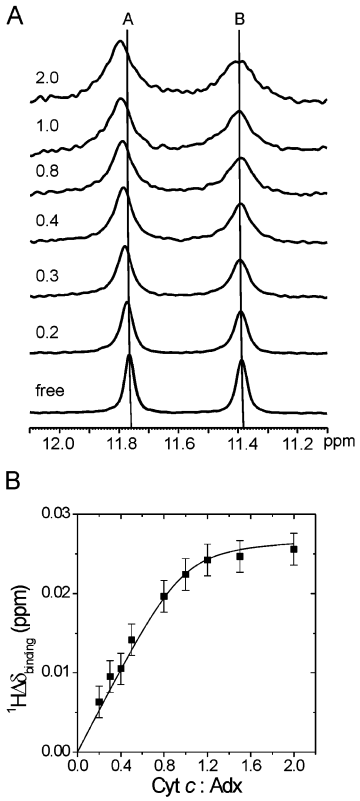

FIGURE 7: 1D ^{1}H NMR data for the titration of ferrous cyt *c* into *wt* Adx (20 mM potassium phosphate at pH 7.4 and 285 K). (A) Downfield-shifted signals of (A) $H_{\delta 1}$ of His56 and (B) H_γ of Ser88 for *wt* Adx in the absence (free) and with an increasing ratio of ferrous cyt *c* and Adx. (B) Titration curve for $H_{\delta 1}$ of His56 upon addition of ferrous cyt *c*, fitted using a 1:1 complex model with a K_a of $(4 \pm 3) \times 10^4$ M^{-1}.

terpredoxin where it is an Arg) and immediately follows the third cysteinyl ligand coordinating the iron−sulfur cluster. Furthermore, it is central to a network of hydrogen bonds that extends throughout the recognition domain.

Upon addition of cyt *c*, $H_{\delta 1}$ of His56 shifts to a downfield position, whereas H_γ of Ser88 is unaffected (Figure 7A). The $\Delta\delta_{binding}$ values plotted as a function of the molar ratio of cyt *c* and Adx can be fitted to a 1:1 binding model, with a K_a of $(4 \pm 3) \times 10^4$ M^{-1}, in agreement with the binding constant from the 2D experiments. In principle, the chemical shift perturbation of a histidine proton could arise from a pH change during the titration. However, the working pH was 7.4, and the pK_a of His56 $H_{\delta 1}$ is <5 (*50*). Furthermore, during the four titration experiments, the pH was monitored throughout, and the perturbation of $H_{\delta 1}$ of His56 to a downfield position was always consistent and follows, within error, a binding curve with the expected K_a. For these reasons, it is reasonable to attribute the shift to formation of a complex.

DISCUSSION

It has been proposed that transient protein complexes can range from well-defined to highly dynamic (*8*, *10*). At one end of the scale, the partners bind in a specific (single) orientation for a large fraction of the lifetime of the complex, utilizing both electrostatic and hydrophobic interactions. For this type of interaction, the $\Delta\delta_{binding}$ is large for polar and hydrophobic residues, which may be a consequence of desolvation upon complex formation. In these complexes, the interface is well-defined and they are amenable to structure determination in solution, as has been demonstrated for cyt *f* and Pc from both higher plants and *Phormidium laminosum* (*51*, *52*).

At the other end of the scale, there is no specific orientation but rather a dynamic ensemble of orientations governed predominantly by electrostatics. In such dynamic complexes, the apparent lack of surface matching allows more than one orientation within a binding domain to be sampled. These orientations would most likely have similar energies and be in fast exchange, resulting in averaging of chemical shift perturbations over all orientations. In combination with the absence of close contacts and extensive desolvation, this would explain the smaller chemical shift perturbations in these complexes and the more extensive binding sites. This is appreciated in Figure 8 (panels A and B) with plots of $\Delta\delta_{avg}$ for cyt *c* in complex with C*c*P (*34*) and for cyt b_5 in complex with Mb (*10*), respectively. The latter complex is much more dynamic (*9*, *12*−*14*), and demonstrates much smaller $\Delta\delta_{avg}$ values overall.

The chemical shift mapping study on cyt *c* in complex with its physiological partner C*c*P (*34*) indicated a binding site encompassing the whole of the front face of the cyt *c* molecule (Figure 9A). The large chemical shift changes (≥0.08 ppm) for polar and hydrophobic residues (T12, Q16, V28, and F82) most likely arise due to short-range interactions pulling the complex into a single orientation for a significant fraction of the complex lifetime. This binding site in solution agrees with the one observed in the crystal state (*53*). In a complex with a nonphysiological partner, cyt *f*, the binding site on cyt *c* was similar though less extensive and two cyt *c* molecules were found to bind to cyt *f* (*11*). In a complex with another nonphysiological partner, Pc, a highly delocalized binding site on cyt *c* was observed, suggesting the complex existed as a dynamic ensemble (*7*) as appears to be the case with a physiological partner flavocytochrome b_2, as determined from kinetic and molecular modeling studies (*54*). In a complex with Adx, the binding site on cyt *c* is less extensive and the average $\Delta\delta_{binding}$ values are somewhat smaller than those of the cyt *c*−C*c*P complex (Figure 8A,C and Figure 9). Nevertheless, the largest chemical shift changes are located around the heme edge, suggesting a predominant site of interaction for Adx, and to a lesser extent an interaction with other parts on the cyt *c* surface. In particular, in the complex with *wt* Adx, residues on the back side of cyt *c* show more extensive perturbations than with Adx(4−108). It is tempting to ascribe this to interactions with the flexible tail of *wt* Adx, which also demonstrates perturbations, but this remains speculative.

For [^{15}N]Adx, the $\Delta\delta_{avg}$ values are similar in magnitude to those observed for cyt *c* (Figure 8D), with an even distribution of charged, polar, and hydrophobic residues being affected upon interaction with cyt *c*. The dominating binding site is located around the negative patch of the recognition domain. This electrostatic interaction is not surprising considering the net charges at neutral pH, +8 for cyt *c* and −8 for *wt* Adx. Like in the case of cyt *c*, however, the interactions are quite dispersed, suggesting that cyt *c* samples a large area of the Adx surface. The dispersion appears to be strongest for Adx(4−108), particularly in the recognition domain where a much broader region appears

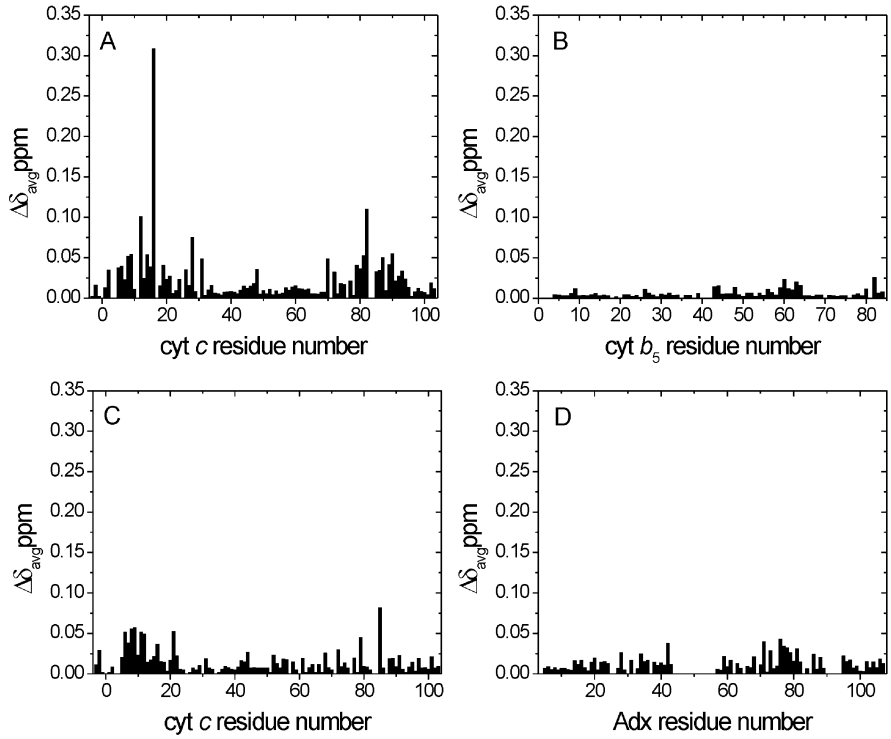

FIGURE 8: Average amide chemical shift plots (at 100% bound) for transient complexes plotted against the respective residue number of the ^{15}N-labeled protein. (A) [^{15}N]Cyt *c*(Fe^{II})−C*c*P(Fe^{III}) complex from yeast, in 20 mM sodium phosphate in which I = 100 mM (NaCl) at pH 6.0 and 313 K with a K_a of ~2 × 10^5 M^{-1} (*34*) (B) [^{15}N]Cyt b_5(Fe^{III})−metMb(Fe^{III}) complex from bovine, in 10 mM potassium phosphate at pH 6.0 and 300 K with a K_a of 5 × 10^3 M^{-1} (*10*). (C and D) [^{15}N]Cyt *c*(Fe^{II})−*wt* Adx(Fe^{III}Fe^{III}) and cyt *c*(Fe^{II})−[^{15}N]*wt* Adx(Fe^{III}Fe^{III}) complexes from yeast and bovine, respectively, in 20 mM potassium phosphate at pH 7.4 and 285 K with a K_a of 4 × 10^4 M^{-1} (this work).

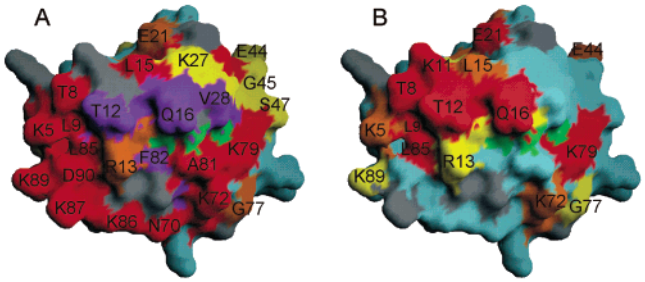

FIGURE 9: Comparison of the chemical shift maps for 100% bound yeast cyt *c* in complex with its physiological partner yeast C*c*P (A) and with the nonphysiological partner bovine *wt* Adx (B). Color coding is the same as in Figure 3, with purple representing chemical shift changes of ≥0.08 ppm.

to be affected compared to a more localized area for *wt* Adx (Figure 5). Furthermore, although chemical shift changes are observed for both forms of Adx in the core domain, they are larger in this region for Adx(4−108). It should be noted that the lack of data on the iron−sulfur binding region and the C-terminal tail in *wt* Adx results in an incomplete picture of the binding map for cyt *c* on Adx.

The peptide strand on Adx, which has been proposed to bind to the partner proteins of Adx, AdR, and cytochromes P450, stretches from residues 45−56 and 65−80 (*15*, *55*). From the study presented here, it is apparent that the backbone amides of these residues are nearly all affected in the presence of cyt *c*. Furthermore, the presence of several strongly affected residues in the core domain, particularly V34, D39, D41, and G42, provides convincing evidence that cyt *c* also samples this surface region. This region has been implicated in cytochrome P450cam (CYP101) binding by the homologous bacterial ferredoxin, putidaredoxin (*56*, *57*), and more recently, the crystal structure of the cross-linked AdR−Adx complex has shown that this region of Adx is in contact with the surface of the reductase (*19*).

The crystal structure of Adx shows that His56 sits in a hollow behind the active site and is surrounded by the side chains of Pro108 and Tyr82 (*18*, *48*). The location of His56 suggests that the hydrophobic patch surrounding the iron−sulfur cluster is affected upon complex formation, with His56 sensing the cyt *c* binding rather than being directly involved. This would be in agreement with results from kinetic studies with His56 mutants where it was postulated that His56 plays only an indirect role in binding redox partners (*58*). This evidence supports the previously proposed view that His56 acts as a communicative link between the active site in the core domain and the residues in the recognition domain required for binding a partner (*49*).

In conclusion, the complex of Adx and cyt *c* demonstrates dominant binding sites at the negative patch in the recognition domain and the heme edge region, respectively. The chemical shift perturbation maps, in combination with the similar size of the chemical shift perturbations both for polar and hydrophobic and for charged residues, indicate that the complex is dynamic, with both proteins sampling other surface areas away from the predominate binding sites. These features further serve to highlight that surface complementarity is relatively unimportant in transient complexes. Finally, the cyt *c*−Adx complex can be placed between complexes with well-defined binding sites such as the cyt *c*−C*c*P complex (*34*) and highly dynamic complexes such as the cyt b_5−Mb complex (*10*).

ACKNOWLEDGMENT

J.A.R.W. is indebted to Dr. P. B. Crowley and Professor G. W. Canters for many useful discussions. We express our gratitude to Dr. F. Hannemann for critical reading of the manuscript.

SUPPORTING INFORMATION AVAILABLE

Amide assignments of *wt* Adx and Adx(4−108) at pH 7.4 and 285 K (Table S1) and a list of the average amide chemical shift changes for cyt *c* and Adx upon complex formation (Table S2). This material is available free of charge via the Internet at http://pubs.acs.org.

REFERENCES

1. Bendall, D. S. (1996) Interprotein Electron Transfer, in *Protein Electron Transfer* (Bendall, D. S., Ed.) pp 43−68, BIOS Scientific Publishers, Oxford, U.K.
2. Chapman, S. K., Knox, C. V., and Sykes, A. G. (1984) Kinetic studies on 1:1 electron-transfer reactions involving blue copper proteins. Part 10. The assignment of binding sites in the reactions of plastocyanin (and azurin) with non-physiological protein redox partners, *J. Chem. Soc., Dalton Trans.*, 2775−2780.
3. Modi, S., He, S. P., Gray, J. C., and Bendall, D. S. (1992) The role of surface exposed Tyr-83 of plastocyanin in electron-transfer form cytochrome *c*, *Biochim. Biophys. Acta 1101*, 64−68.
4. Peerey, L. M., and Kostic, N. M. (1989) Oxidoreduction reactions involving the electrostatic and the covalent complex of cytochrome *c* and plastocyanin: importance of the protein rearrangement for the intracomplex electron-transfer reaction, *Biochemistry 28*, 1861−1868.
5. Zhou, J. S., and Kostic, N. M. (1992) Photoinduced electron-transfer from zinc cytochrome *c* to plastocyanin is gated by surface-diffusion within the metalloprotein complex, *J. Am. Chem. Soc. 114*, 3562−3563.
6. Pletneva, E. V., Fulton, D. B., Kohzuma, T., and Kostic, N. M. (2000) Protein docking and gated electron-transfer reactions between zinc cytochrome *c* and the new plastocyanin from the fern *Dryopteris crassirhizoma*. Direct kinetic evidence for multiple binary complexes, *J. Am. Chem. Soc. 122*, 1034−1046.
7. Ubbink, M., and Bendall, D. S. (1997) Complex of plastocyanin and cytochrome *c* characterized by NMR chemical shift analysis, *Biochemistry 36*, 6326−6335.
8. Crowley, P. B., Vintonenko, N., Bullerjahn, G. S., and Ubbink, M. (2002) Plastocyanin-cytochrome *f* interactions: The influence of hydrophobic patch mutations studied by NMR spectroscopy, *Biochemistry 41*, 15698−15705.
9. Liang, Z. X., Nocek, J. M., Huang, K., Hayes, R. T., Kurnikov, I. V., Beratan, D. N., and Hoffman, B. M. (2002) Dynamic docking and electron transfer between Zn-myoglobin and cytochrome b_5, *J. Am. Chem. Soc. 124*, 6849−6859.
10. Worrall, J. A. R., Liu, Y., Crowley, P. B., Nocek, J. M., Hoffman, B. M., and Ubbink, M. (2002) Myoglobin and cytochrome b_5: A nuclear magnetic resonance study of a highly dynamic protein complex, *Biochemistry 41*, 11721−11730.
11. Crowley, P. B., Rabe, K. S., Worrall, J. A. R., Canters, G. W., and Ubbink, M. (2002) The ternary complex of cytochrome *f* and cytochrome *c*: Identification of a second binding site and competition for plastocyanin binding, *ChemBioChem 3*, 526−533.
12. Liang, Z. X., Nocek, J. M., Kurnikov, I. V., Beratan, D. N., and Hoffman, B. M. (2000) Electrostatic control of electron transfer between myoglobin and cytochrome b_5: Effect of methylating the heme propionates of Zn-myoglobin, *J. Am. Chem. Soc. 122*, 3552−3553.
13. Liang, Z. X., Jiang, M., Ning, Q., and Hoffman, B. M. (2002) Dynamic docking and electron transfer between myoglobin and cytochrome b_5, *J. Biol. Inorg. Chem. 7*, 580−588.
14. Furukawa, Y., Matasuda, F., Ishimori, K., and Morishima, I. (2002) Investigation of the electron-transfer mechanism by cross-linking between Zn-substituted myoglobin and cytochrome b_5, *J. Am. Chem. Soc. 124*, 4008−4019.
15. Grinberg, A. V., Hannemann, F., Schiffler, B., Müller, J., Heinemann, U., and Bernhardt, R. (2000) Adrenodoxin: structure, stability, and electron transfer properties, *Proteins 40*, 590−612.
16. Bernhardt, R. (1996) Cytochrome P450: structure, function, and generation of reactive oxygen species, *Rev. Physiol., Biochem. Pharmacol. 127*, 137−221.
17. Miura, S., and Ichikawa, Y. (1991) Proton nuclear magnetic resonance investigation of adrenodoxin. Assignment of aromatic resonances and evidence for a conformational similarity with ferredoxin from *Spirulina platensis*, *Eur. J. Biochem. 197*, 747−775.
18. Pikuleva, I. A., Tesh, K., Waterman, M. R., and Kim, Y. (2000) The tertiary structure of full-length bovine adrenodoxin suggests functional dimers, *Arch. Biochem. Biophys. 373*, 44−55.
19. Müller, J. J., Lapko, A., Bourenkov, G., Ruckpaul, K., and Heinemann, U. (2001) Adrenodoxin reductase-adrenodoxin complex structure suggests electron transfer path in steroid biosynthesis, *J. Biol. Chem. 276*, 2786−2789.
20. Cupp, J. R., and Vickery, L. E. (1989) Adrenodoxin with a COOH-terminal deletion (des 116−128) exhibits enhanced activity, *J. Biol. Chem. 264*, 1602−1607.
21. Uhlmann, H., Kraft, R., and Bernhardt, R. (1994) C-terminal region of adrenodoxin affects its structural integrity and determines differences in its electron transfer function to cytochrome *P*-450, *J. Biol. Chem. 269*, 22557−22564.
22. Omura, T., Sanders, E., and Estabrook, R. W. (1966) Isolation from adrenal cortex of a nonheme iron protein and a flavoprotein functional as a reduced triphospyridine nucleotide-cytochrome P-450 reductase, *Arch. Biochem. Biophys. 117*, 660−673.
23. Lambeth, J. D., Seybert, D. W., and Kamin, H. (1979) Ionic effects in adrenal steroidogenic electron transport, *J. Biol. Chem. 254*, 7255−7264.
24. Geren, L. M., O'Brien, P., Stoneheuerner, J., and Millet, F. (1984) Identification of specific carboxylate groups on adrenodoxin that are involved in the interaction with adrenodoxin reductase, *J. Biol. Chem. 259*, 2155−2160.
25. Coghlan, V. M., and Vickery, L. E. (1991) Site-specific mutations in human ferredoxin that affect binding to ferredoxin reductase and cytochrome P450scc, *J. Biol. Chem. 266*, 18606−18612.
26. Lambeth, J. D., and Kamin, H. (1979) Adrenodoxin reductase: adrenodoxin complex Flavin to iron−sulfur transfer as the rate-limiting step in the NADPH-cytochrome *c* reductase reaction, *J. Biol. Chem. 254*, 2766−2774.
27. Zuiderweg, E. R. P. (2002) Mapping protein−protein interactions in solution by NMR spectroscopy, *Biochemistry 41*, 1−7.
28. Guiles, R. D., Sarma, S., DiGate, R. J., Banville, D., Basus, V. J., Kuntz, I. D., and Waskell, L. (1996) Pseudocontact shifts used in the restraint of the solution structures of electron transfer complexes, *Nat. Struct. Biol. 3*, 333−339.
29. Morelli, X., Dolla, A., Czjek, M., Palma, P. N., Blasco, F., Krippahl, L., Moura, J. J. G., and Guerlesquin, F. (2000) Heteronuclear NMR and soft docking: An experimental approach for a structural model of the cytochrome *c*(553)-ferredoxin complex, *Biochemistry 39*, 2530−2537.
30. Hom, K., Ma, Q. F., Wolfe, G., Zhang, H., Storch, E. M., Daggett, V., Basus, V. J., and Waskell, L. (2000) NMR studies of the association of cytochrome b_5 with cytochrome *c*, *Biochemistry 39*, 14025−14039.
31. Hall, D. A., Kooi, C. W. V., Stasik, C. N., Stevens, S. Y., Zuiderweg, E. R. P., and Matthews, R. G. (2001) Mapping the interactions between flavodoxin and its physiological partners flavodoxin reductase and cobalamin-dependent methionine synthase, *Proc. Natl. Acad. Sci. U.S.A. 98*, 9521−9526.
32. Arnesano, F., Banci, L., Bertini, I., Cantini, F., Ciofi-Baffoni, S., Huffman, D. L., and O'Halloran, T. V. (2001) Characterization of the binding interface between the copper chaperone Atx1 and the first cystolic domain of Ccc2 ATPase, *J. Biol. Chem. 276*, 41365−41376.
33. Crowley, P. B., Diáz-Quintana, A., Molina-Heredia, F. P., Nieto, P., Sutter, M., Haehnel, W., De la Rosa, M., and Ubbink, M. (2002) The interactions of cyanobacterial cytochrome c_6 and cytochrome *f*: Characterized by NMR, *J. Biol. Chem. 277*, 48685−48689.
34. Worrall, J. A. R., Kolczak, U., Canters, G. W., and Ubbink, M. (2001) Interaction of yeast iso-1-cytochrome *c* with cytochrome *c* peroxidase investigated by [^{15}N,^{1}H] heteronuclear NMR spectroscopy, *Biochemistry 40*, 7069−7076.
35. Pollock, W. B. R., Rosell, F. I., Twitchett, M. B., Dumont, M. E., and Mauk, A. G. (1998) Bacterial expression of mitochondrial cytochrome *c*. Trimethylation of Lys72 in yeast iso-1-cytochrome *c* and the alkaline conformational transition, *Biochemistry 37*, 6124−6131.

36. Morar, A. S., Kakouras, D., Young, G. B., Boyd, J., and Pielak, G. J. (1999) Expression of ^{15}N-labeled eukaryotic cytochrome *c* in *Escherichia coli*, *J. Biol. Inorg. Chem. 4*, 220−222.
37. Margoliash, E., and Frohwirt, N. (1959) Spectrum of horse-heart cytochrome *c*, *Biochem. J. 71*, 570−572.
38. Kimura, T. (1968) Biochemical aspects of iron−sulfur linkage in non-heme iron proteins, with special reference to "adrenodoxin", *Struct. Bonding 5*, 1−40.
39. Kraulis, P. J. (1989) ANSIG: A program for the assignment of protein ^{1}H 2D-NMR spectra by interactive computer-graphics, *J. Magn. Reson. 84*, 627−633.
40. Kraulis, P. J., Domaille, P. J., Campbell-Burk, S. L., Van Aken, T., and Laue, E. D. (1994) Solution structure and dynamics of Ras P21-center-DOT-GDP determined by heteronuclear 3-Dimensional and 4-Dimensional NMR spectroscopy, *Biochemistry 33*, 3515−3531.
41. Weiss, R., Brachais, L., Löhr, F., Hartleib, J., Bernhardt, R., and Rüterjans, H. (2000) Assignment of ^{1}H, ^{13}C and ^{15}N signals of bovine adrenodoxin, *J. Biomol. NMR 17*, 355−356.
42. Andersson, P., Gsell, B., Wipf, B., Senn, H., and Otting, G. (1998) HMQC and HSQC experiments with water flip-back optimized for large proteins, *J. Biomol. NMR 11*, 278−288.
43. Kannt, A., Young, S., and Bendall, D. S. (1996) The role of acidic residues of plastocyanin in its interaction with cytochrome *f*, *Biochim. Biophys. Acta 1277*, 115−126.
44. Garrett, D. S., Seok, Y. J., Liao, D. I., Peterkofsky, A., Gronenborn, A. M., and Clore, G. M. (1997) Solution structure of the 30 kDa N-terminal domain of enzyme I of the *Escherichia coli* phosphoenolpyruvate:sugar phosphotransferase system by multidimensional NMR, *Biochemistry 36*, 2517−2530.
45. Bertini, I., Luchinat, C., and Rosato, A. (1999) NMR spectra of iron−sulfur proteins, *Adv. Inorg. Chem. 47*, 251−282.
46. Louie, G. V., and Brayer, G. D. (1990) High-resolution refinement of yeast iso-1-cytochrome *c* and comparisons with other eukaryotic cytochromes *c*, *J. Mol. Biol. 214*, 527−555.
47. Nicholls, A., Sharp, K., and Honig, B. (1991) Protein folding and association: insights from the interfacial and thermodynamic properties of hydrocarbons, *Proteins 11*, 281−296.
48. Müller, A., Müller, J. J., Muller, Y. A., Uhlmann, H., Bernhardt, R., and Heinemann, U. (1998) New aspects of electron transfer revealed by the crystal structure of a truncated bovine adrenodoxin, Adx(4−108), *Structure 6*, 269−280.
49. Kostic, M., Pochapsky, S. S., Obenauer, J., Mo, H., Pagani, G. M., Pejchal, R., and Pochapsky, T. C. (2002) Comparison of functional domains in vertebrate-type ferredoxins, *Biochemistry 41*, 5978−5989.
50. Xia, B., Volkman, B. F., and Markley, J. L. (1998) Evidence for oxidation-state-dependent conformational changes in human ferredoxin from multinuclear, multidimensional NMR spectroscopy, *Biochemistry 37*, 3965−3973.
51. Ubbink, M., Ejdeback, M., Karlsson, B. G., and Bendall, D. S. (1998) The structure of the complex of plastocyanin and cytochrome *f*, determined by paramagnetic NMR and restrained rigid-body molecular dynamics, *Structure 6*, 323−335.
52. Crowley, P. B., Otting, G., Schlarb-Ridley, B. G., Canters, G. W., and Ubbink, M. (2001) Hydrophobic interactions in a cyanobacterial plastocyanin-cytochrome *f* complex, *J. Am. Chem. Soc. 123*, 10444−10453.
53. Pelletier, H., and Kraut, J. (1992) Crystal structure of a complex between electron transfer partners, cytochrome *c* peroxidase and cytochrome *c*, *Science 258*, 1748−1755.
54. Short, D. M., Walkinshaw, M. D., Taylor, P., Reid, G. A., and Chapman, S. K. (1998) Location of a cytochrome *c* binding site on the surface of flavocytochrome b_2, *J. Biol. Inorg. Chem. 3*, 246−252.
55. Hannemann, F., Rottmann, M., Schiffler, B., and Bernhardt, R. (2001) The loop region covering the iron−sulfur cluster in bovine adrenodoxin comprises a new interaction site for redox partners, *J. Biol. Chem. 276*, 1369−1375.
56. Pochapsky, T. C., Lyons, T. A., Kazanis, S., Arakaki, T., and Ratnaswamy, G. (1996) A structure-based model cytochrome for cytochrome $P450_{cam}$-putidaredoxin interactions, *Biochimie 78*, 723−733.
57. Roitberg, A. E., Holden, M. J., Mayhew, M. P., Kurnikov, I. V., Beratan, D. N., and Vilker, V. L. (1998) Binding and electron transfer between putidaredoxin and cytochrome $P450_{cam}$. Theory and experiments, *J. Am. Chem. Soc. 120*, 8927−8932.
58. Beckert, V., Schrauber, H., Bernhardt, R., Van Dijk, A. A., Kakoschke, C., and Wray, V. (1995) Mutational effects on the spectroscopic properties and biological activities of oxidized bovine adrenodoxin, and their structural implications, *Eur. J. Biochem. 231*, 226−235.

BI0342968